

# Dye removal using 4A-zeolite/polyvinyl alcohol mixed matrix membrane adsorbents: preparation, characterization, adsorption, kinetics, and thermodynamics

Bahareh Baheri<sup>1</sup> · Raziye Ghahremani<sup>1</sup> ·  
Mohammad Peydayesh<sup>1</sup> · Mahnaz Shahverdi<sup>1</sup> ·  
Toraj Mohammadi<sup>1</sup>

Received: 22 August 2015 / Accepted: 12 November 2015 / Published online: 24 November 2015  
© Springer Science+Business Media Dordrecht 2015

**Abstract** In pursuit of improving performance of the methylene blue adsorption process, the potential of a novel 4A-zeolite/polyvinyl alcohol (PVA) membrane adsorbent was investigated. Adding 4A-zeolite particles to the PVA membrane adsorbent provided an effective structure for the adsorptive membrane in dye removal processes. Effect of zeolite content was also studied via synthesis of different mixed matrix membrane adsorbents (MMMAs) with 5, 10, 15, and 20 wt% 4A-zeolite content. Morphology of MMMA was analyzed by scanning electron microscope and the intermolecular interactions were determined by Fourier transform infrared spectroscopy. X-ray diffraction was performed to determine the crystal structure of MMMA. For the sake of finding optimum condition, the adsorption capacity was examined at various operating parameters, such as contact time, temperature, pH, and initial concentration. The maximum value of the adsorption capacity ( $q_e$ ) of 41.08 mg g<sup>-1</sup> and the highest removal efficiency of 87.41 % were obtained by applying 20 wt% loading of 4A-zeolite. The experimental data were fitted well with the Freundlich adsorption isotherm model ( $R^2 = 0.9917$ ) compared with the Langmuir ( $R^2 = 0.9489$ ) and the Tempkin ( $R^2 = 0.8886$ ) adsorption isotherm models, and the adsorption kinetic data verified the best fitting with the pseudo-second-order model ( $R^2 = 0.9999$ ). The estimated data for Gibb's free energy ( $\Delta G^\circ$ ) showed that the adsorption process is spontaneous at lower temperature values and non-spontaneous at higher temperature values. Other evaluated thermodynamic parameters such as changing in enthalpy ( $\Delta H^\circ$ ) and entropy ( $\Delta S^\circ$ ) revealed that the adsorption process is exothermic with an increase in orderliness at the solid/solution interface.

---

✉ Toraj Mohammadi  
torajmohammadi@iust.ac.ir

<sup>1</sup> Research and Technology Centre of Membrane Processes, Faculty of Chemical Engineering, Iran University of Science and Technology (IUST), Narmak, Tehran, Iran

**Keywords** Membrane adsorbent · Dye removal · 4A-zeolite · PVA · MB

## Introduction

The world today is faced with challenging and multifaceted issues in huge production of industrial and domestic effluents, which have led to the pollution of the earth's water and soil and is potentially irreversibly harmful for the flora and fauna. This developing situation has inevitably led scientists to keep up with pressing demands for a rising wider range of ideas and new technologies. Dyestuff and heavy metal ions are the prominent pollutant constituents of industrial waste water, and are produced from variety of industries such as textile, plastic, varnish and paint, printing, ink, chemical manufacturing, tannery, and mining. Dyes are not only the most apparent signal of water pollution, but also most dyes are tenacious organic molecules resistant to heat, sunlight, and oxidizing agents; additionally, they can affect the amount of sunlight penetrating water surface and reduce photosynthetic activities. Therefore, discarding dyes into streams, lakes, and oceans can change the biological life of aquatic flora and micro-organisms [1–4].

Methylene blue (MB) is a heterocyclic aromatic cationic dye, which has numerous uses in varying areas such as biology and chemistry [5, 6]. Although cationic dyes are usually used in different purposes due to their durability and suitability, they possess several adverse effects and they have to be eliminated from the wastewater streams [7].

Various techniques are employed to remove dye from industrial effluent divided into three categories: chemical, physical, and biological methods. The chemical methods usually use oxidative processes such as ozonation, photochemical, electrochemical destruction, cucurbituril, and sodium hypochlorite, while in most cases hydrogen peroxide is used, and it has to be activated. The physical methods comprise adsorption, membrane filtration, and ion exchange. Adsorption techniques with activated carbon, peat, wood chips, fly ash and coal, silica gel, and electrokinetic coagulation are widely used today [8–10]. All of these techniques have their advantages and disadvantages. The prominent impediment in transforming most of these methods from lab-scale to industry is cost. The best way to overcome the problem is combination of these methods to employ them in their best performance [11].

The adsorption process and membrane filtration are two fundamental and effective strategies to remove dyes from wastewater because of their simple design and operation, economical cost, and resistance to toxic materials [12]. Membrane technology can continuously separate dye from effluent and industrial wastewater and has some exceptional ability unrivalled by other methods, such as resistance to temperature, adverse chemical environments, and microbial attack [11]. Ion-exchange systems, clarifiers, deaerators, and wastewater bioreactors can be replaced by membrane techniques [13].

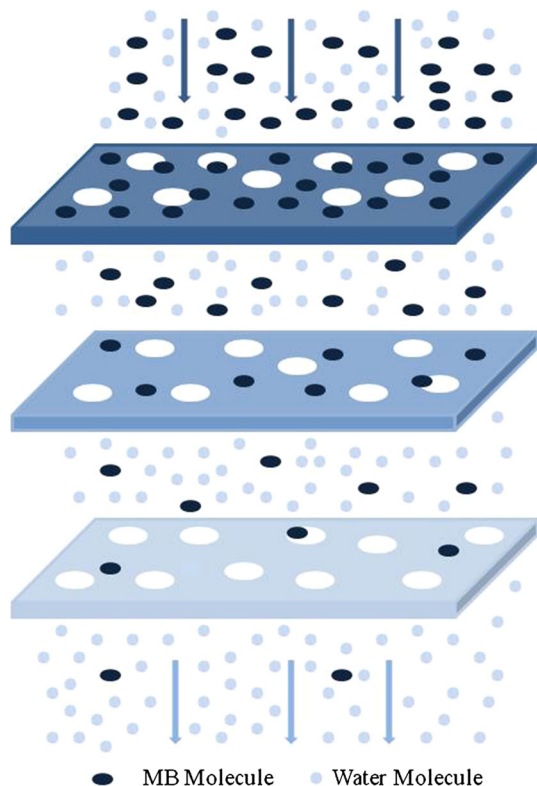
A combination of membrane technology with adsorption results in a new developing field called membrane adsorption [14]. This can be investigated in two ways, including preparing the membrane as merely an adsorbent (batch method) and

enhancing membrane property for adsorbing target material in membrane processes (flow-through method). Hence, they can be used in batch or flow-through methods (Fig. 1). The membrane adsorption technology offers a fast and convenient alternative to column and batch adsorption.

The high void volume structure and elevated surface area, as well as their electrostatic forces towards dye molecules, make zeolites the best candidate for enhancing the adsorption capacity of membranes and improving their performance. Using zeolite particles in polymeric membranes is a promising way to enhance the properties of the membrane adsorbent by imparting both of polymeric and inorganic materials advantages. The presence of variety of favorable results in this occasion indicates the improved functioning of this type of membranes [15, 16]. One of the advantages of applying zeolites in water/wastewater treatment industries, apart from their low cost, is ion selectivity. 4A-zeolite is a synthetic product with a significant adsorptive characteristic, which can be produced economically and is a completely natural ingredient and biodegradable. 4A-zeolite has a high exchange capacity, which makes it a proper candidate for adsorption processes [17].

In this work, a new type of membrane adsorbent was fabricated using polyvinyl alcohol (PVA) filled with 4A-zeolite particles. The effects of various amounts of 4A-zeolite particles content, operation temperature, MB solution concentration, and

**Fig. 1** The schematic view of membrane adsorbent in flow-through method for separating MB from water



pH were investigated in performance of mixed matrix membrane adsorbent (MMMA) for removal of MB from aqueous solutions. The current work is based on determining the properties of this new MMMA and evaluating its adsorption capacity. This MMMA can be fabricated in various shapes and with different porosities depending on its application for using in batch or continuous systems.

## Experimental

### Materials

4A-zeolite (particle size = 300–400 nm, pore size = 3.8 Å, Si/Al molar ratio = 1) was purchased from the Research Institute of Petroleum Industries, Iran. PVA (98 %, molecular weight = 145,000) and glutaraldehyde (GA, 50 wt%) were purchased from Merck. Distilled water was used throughout the research work.

### Membrane preparation

A proper amount of PVA powder was sprinkled slowly into hot, double-distilled water at 95 °C, while it was magnetically stirred strongly to form a 10 wt% polymeric solution. The beaker was covered with plastic wrap and stirred until the solution was cleared. Then, the solution was cooled down to room temperature, and a certain amount of GA as crosslinker (0.05 mol for each mole of monomeric unit) was added to the solution. The 4A-zeolite particles with 5, 10, 15, 20 wt% of the polymer were dispersed in water and sonicated for 1 h (Hilsonic, Birkenhead, UK). The 4A-zeolite was added to the solution and gently stirred at ambient temperature for 2 h. Afterwards, the polymeric solution was casted over a glass plate with the aid of a casting knife. The membranes were placed in a dust free environment at room temperature for 24 h to evaporate the solvent. The dried membranes were heated in an oven and hold at about 150 °C for 1 h to complete the crosslinking reactions [18, 19].

All the membranes were as thick as 50 µm (Mitutoyo Model MDC-25SB digital micrometer, 1 µm accuracy). They were cut into 0.5 × 0.5 cm<sup>2</sup> squarish shape to utilize in the adsorption experiments.

### Adsorption experiments

The batch condition was applied in order to carry out the adsorption experiments. In each experiment, the dried samples of adsorptive membranes were added to the MB solutions in different concentrations, which were prepared by diluting the stock solution (500 mg L<sup>-1</sup>) with an adsorbent dosage of 1 g L<sup>-1</sup>. To adjust the pH, an appropriate amount of diluted sodium hydroxide (NaOH) or hydrogen chloride (HCl) was added to the solutions. The solutions were agitated with a magnetic stirrer at 25 °C and 350 rpm. In order to evaluate the adsorption capacity of 4A-zeolite powder, some experiments were carried out in the same condition as mentioned above and with the same adsorbent dosage. The powder of zeolite was

separated from the solutions using a centrifuge at speed of  $6000 \text{ min}^{-1}$  (Hettich EBA 20).

Dye removal efficiency after the adsorption process was calculated by measuring the concentrations of samples specified at characteristic wavelength of 633 nm using a double beam UV-visible spectrophotometer Shimadzu UV-1800. The amount of dye adsorbed per unit mass of the adsorbent ( $q_e$ ) and the percentage dye removal efficiency ( $R\%$ ) were evaluated using the following equations, respectively:

$$q_e = \frac{(C_0 - C_e)V}{M} \quad (1)$$

$$R\% = \frac{(C_0 - C_e)}{C_0} \times 100 \quad (2)$$

where  $C_0$  and  $C_e$  ( $\text{mg L}^{-1}$ ) are initial and final concentrations of dye,  $V$  (L) is volume of the dye solution and  $M$  (g) is weight of the membrane adsorbent which were used in this research [17]. Figure 2 shows the MMMA and 4A-zeolite powder before and after adsorption experiment.

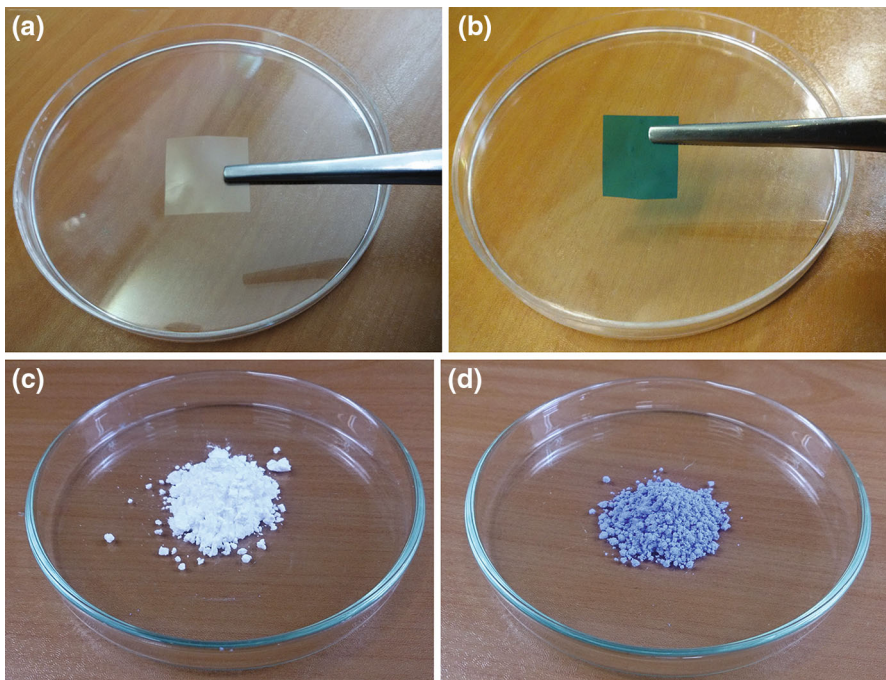


**Fig. 2** Digital image of MMMA before (a) and after (b) adsorption experiments ( $0.5 \times 0.5 \text{ cm}^2$ ) and 4A-zeolite powder before (c) and after (d) adsorption experiments

## Results and discussion

### Morphology and structure characterization of MMMAs

#### SEM analysis

Figure 3 shows surface (a) and cross-sectional (b) scanning electron microscope (SEM) images of MMMAs at 15 wt% zeolite loading at high magnification. The membrane morphology was examined with a CamScan SEM (Model MV2300) microscope. The images obviously exhibit that the 4A-zeolite particles were dispersed finely through the polymer matrix and the main probable defect of voids (at least interconnected macro voids) around incorporated filler particles are not formed during preparation of the MMMAs. It must be mentioned that no surface modifying agent was used in the experiments.

#### FTIR analysis

Fourier transform infrared spectroscopy (FTIR) spectra of the MMMAs before and after MB adsorption are presented in Fig. 4a. The broad adsorption peak observed at  $3310\text{ cm}^{-1}$  corresponds to the O–H stretching vibration of the hydroxyl group of PVA and zeolite. A sharp intense band appearing at around  $1098\text{ cm}^{-1}$  is assigned to the Si–O stretching, and the multiple bands appearing between  $500$  and  $1000\text{ cm}^{-1}$  are assigned to the stretching of Al–O vibrations due to the presence of zeolite. The peak located at  $2924\text{ cm}^{-1}$  is assigned to the stretching vibration of C–H bond. Characteristic changes observed in the FTIR spectrum of MMMAs after the dye adsorption indicate that some peaks are shifted or disappeared, and new peaks are also detected. These changes suggest the MB interactions with the functional groups of the MMMAs in the adsorption process [20].

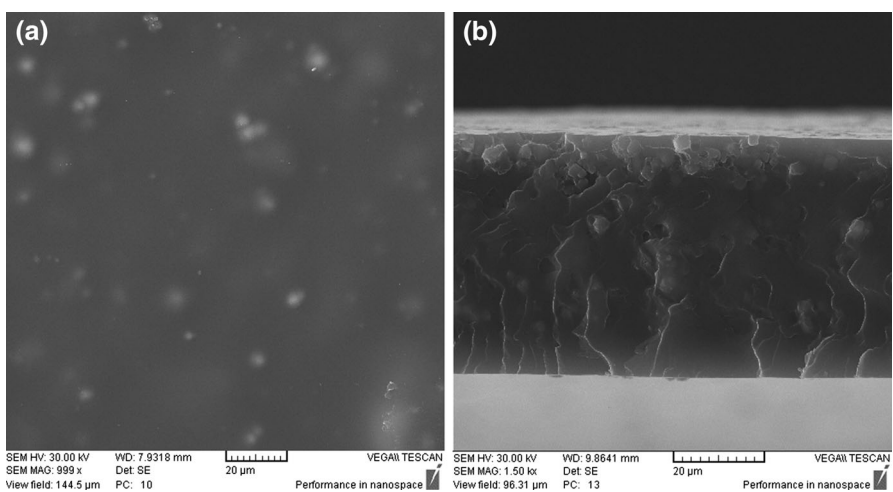


**Fig. 3** Surface (a) and cross-sectional (b) SEM images of the MMA at 15 wt% 4A-zeolite loading

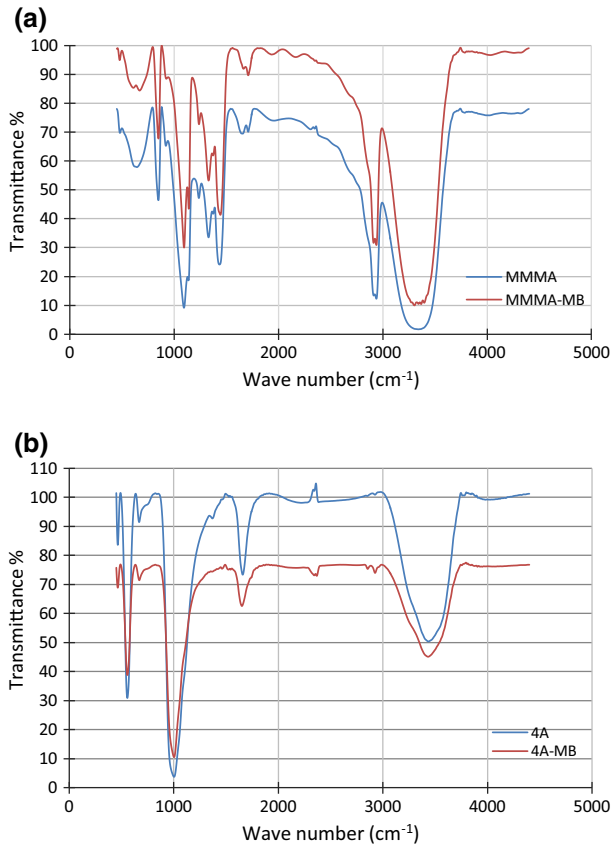


**Fig. 4** FTIR spectra of the MMMA (a) and 4A-zeolite (b) before and after MB adsorption

FTIR of the neat 4A-zeolite powder and MB loaded 4A-zeolite powder are shown in Fig. 4b. As observed, the sharp peak with high intensity at  $1020\text{ cm}^{-1}$  is assigned to the Si–Al–O asymmetric stretching vibration. The band at  $680\text{ cm}^{-1}$  can be assigned to the Si–Al–O symmetric stretching and has less intensity compared with the asymmetric stretching of Si–Al–O bond. Another sharp and intense band at  $564\text{ cm}^{-1}$  is related to the presence of the double four-rings in 4A-zeolite framework structure. Comparison between two FTIR spectra before and after adsorption shows that some peaks are transferred and their intensities are changed. These changes verify the MB interactions with the functional groups of 4A-zeolite [21].

#### *XRD analysis*

To verify crystal structure of the samples, X-ray diffraction (XRD) was performed with an INEL model EQUINOX 3000 (France) X-ray diffractometer using Cu K $\alpha$  X radiation. XRD patterns of the neat polymeric membrane and the MMMA with 20

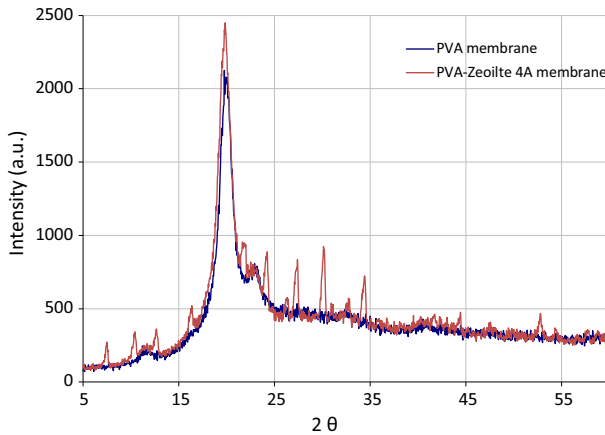


**Fig. 5** XRD pattern of the neat PVA membrane and the MMA with 20 wt% 4A-zeolite loading

wt% 4A-zeolite loading are presented in Fig. 5. In comparison with the neat PVA membrane, some new peaks are observed. The existence of the zeolite crystals in the MMA makes peaks sharper representing more crystalline structure.

### Effect of 4A-zeolite loading on MB adsorption

To improve the dye removal performance by the PVA membrane adsorbent appropriately, some tests were carried out by adding different content of 4A-zeolite particles to the PVA to form different MMAs. The results are presented in Fig. 6. It was revealed that increasing the 4A-zeolite content from 5 to 20 wt% increases the adsorption capacity from 7.10 to 9.18 mg g<sup>-1</sup> and the MB percentage removal efficiency from 61.98 to 80.17 % at temperature of 25 °C, pH of 8.5 and MB concentration of 10 mg L<sup>-1</sup>. As observed, mixing the membrane adsorbent with 4A-zeolite particles provides an effective structure which leads to the higher dye removal. This phenomenon could be related to introducing functional groups of zeolite such as silanol groups to the polymeric membrane, which has stronger affinity for adsorbing cationic dye molecules and leads to stronger electrostatic interaction between MMAs and MB [22]. Therefore, the porous 4A-zeolite powder, which individually has high affinity to adsorb MB, gives special characteristics to the dense polymeric matrix and improves its specific surface area and thus its adsorption capacity.

### Effect of contact time on MB adsorption

As observed in Fig. 7, after 180 min, the adsorption process reaches equilibrium. This behavior can be clarified as a two-step kinetic conduct, a quick initial adsorption followed by a slow adsorption. The huge affinity between MB molecules and the MMAs causes a rapid dye adsorption rate at the first 25 min. It is noteworthy that the abundance of adsorbent vacant sites at the beginning of the



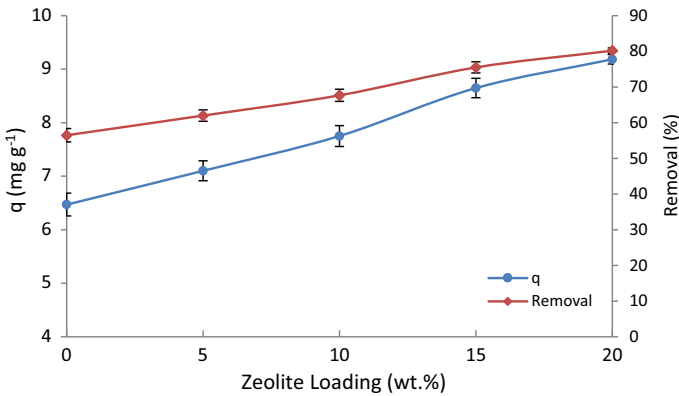
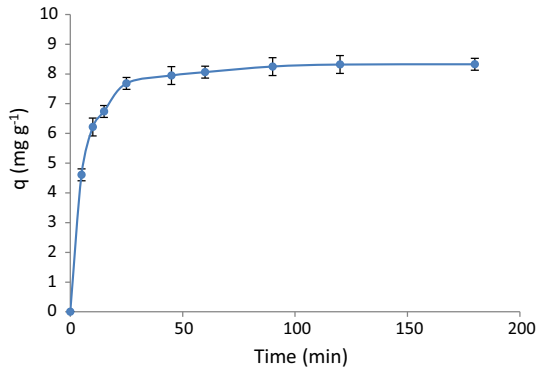


**Fig. 6** Effect of the zeolite loading on MB adsorption at pH of 8.5, initial MB concentration of  $10 \text{ mg L}^{-1}$ , temperature of  $25 \text{ }^\circ\text{C}$  and contact time of 180 min

**Fig. 7** Effect of contact time on MB adsorption at pH of 8.5, initial MB concentration of  $10 \text{ mg L}^{-1}$ , temperature of  $25 \text{ }^\circ\text{C}$



adsorption process leads to a high solute concentration gradient. Formation of the probable monolayer of dye on the MMMA's surface and reduction of the unoccupied sites of adsorbent by approaching the equilibrium time decline the adsorption rate [23].

### Effect of temperature on MB adsorption

In order to analyze the effect of temperature, adsorption experiments were performed at 25, 35, 45, 55, and  $65 \text{ }^\circ\text{C}$ . As observed in Fig. 8, by increasing temperature from 25 to  $65 \text{ }^\circ\text{C}$  the adsorption capacity decreases from  $9.22$  to  $1.46 \text{ mg g}^{-1}$  and the removal efficiency declines from 80.57 to 12.98 % at pH of 8.5, MB concentration of  $10 \text{ mg L}^{-1}$  and 20 wt% 4A-zeolite loading. The greatest adsorption capacity was obtained at  $25 \text{ }^\circ\text{C}$ , confirming the less interaction between MB and the active chemical groups of MMMA at higher temperature. It

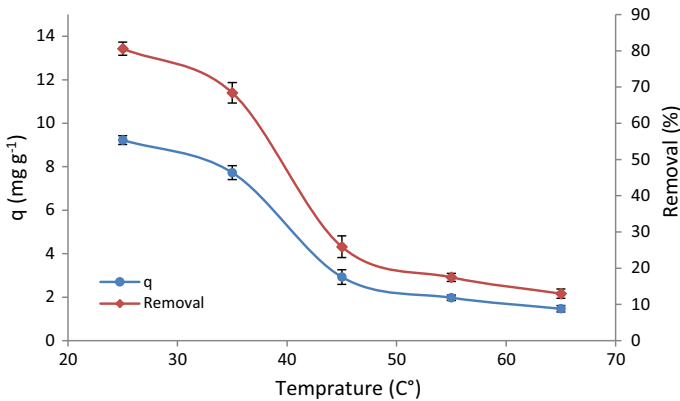


**Fig. 8** Effect of temperature on MB adsorption at pH of 8.5, initial MB concentration of  $10 \text{ mg L}^{-1}$ , and contact time of 180 min

demonstrates that the adsorption process of MB molecules onto the MMMA is exothermic [23].

### Effect of pH solution on MB adsorption

The effect of pH on the MB adsorption using the MMMA as an important controlling parameter is exhibited in Fig. 9. Changing pH affects both the surface charge of MMMA and the ionization degree of MB molecules in the solution [23, 24]. Changing the characteristics of MMMA at different pH values can be explained by two mechanisms: surface charges of PVA chains and 4A-zeolite particles. At higher pH values, deprotonation on the polymer chains releases free

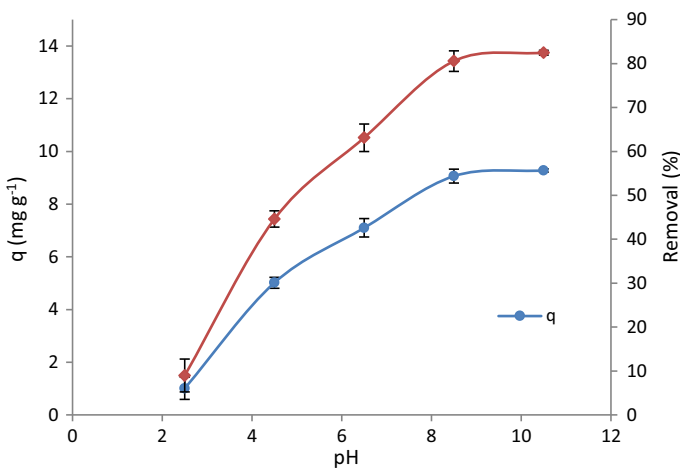


**Fig. 9** Effect of pH on MB adsorption at initial MB concentration of  $10 \text{ mg L}^{-1}$ , temperature of  $25 \text{ }^\circ\text{C}$  and contact time of 180 min

oxygen on its surface which makes a higher inclination of MB positive charged molecules to bind with the MMAs. In contrast, at lower pH values the protonated surface of polymer chains prevents binding the MB molecules with the MMAs [25, 26]. In addition, exposing the zeolite surface to water causes ionization of the surface hydroxyl groups (SiOH and AlOH). The higher selectivity of 4A-zeolite for  $H_3O^+$  ions at the lower pH values causes a competition between  $H_3O^+$  ions and MB molecules for the exchange sites. At higher pH values, the surface functional groups of 4A-zeolite may be dissociated and this leaves more anionic surface sites, which strongly contribute to the MB removal. The isoelectric point of 4A-zeolite is also around 8, so it is positively charged at the pH values lower than 8. The influence of pH can be clearly explained by electrostatic interaction between the MMAs and MB molecules, and it is noticeable that in acidic mediums a reduction in the MB removal appears due to increasing the positively charged groups on 4A-zeolite and polymer chains [27]. By enhancing the pH values from 2.5 to 10.5, the MB adsorption capacity and the MB removal efficiency increase from 1.00 to 9.27 mg g<sup>-1</sup> and 8.97 to 82.49 %, respectively, at temperature of 25 °C, MB concentration of 10 mg L<sup>-1</sup> and 20 wt% 4A-zeolite loading. Besides, due to the strong influence of pH on the electrostatic interaction between 4A-zeolite and cationic dye in the adsorption experiments, the influence of pH on the adsorption capacity of 4A-zeolite particles was also studied, and the results are shown in Table 1.

### Effect of initial MB concentration on MB adsorption

The effect of initial MB concentration on the adsorption experiments is presented in Fig. 10. Apparently, by increasing the initial MB concentration, the adsorption capacity increases. As observed, when the initial MB concentration enhances from 5 to 100 mg L<sup>-1</sup>, the amount of MB adsorbed at equilibrium increases from 4.90 to 41.08 mg g<sup>-1</sup>, while the removal efficiency decreases from 87.41 to 37.35 % at temperature of 25 °C, pH of 10.5 and 20 wt% 4A-zeolite loading. Increasing initial MB concentration leads to the higher mass transfer driving force which causes the greater MB adsorption capacity. However, reduction of the attainable adsorption sites decreases the dye removal efficiency [24, 28].

### Adsorption kinetics

In order to analyze the adsorption kinetic mechanism of transferring MB to the MMAs, pseudo-first-order, pseudo-second-order, and intraparticle diffusion models were applied to fit the experimental data.

**Table 1** Effect of pH on MB adsorption by 4A-zeolite powder at initial MB concentration of 10 mg L<sup>-1</sup>, temperature of 25 °C and contact time of 180 min

pH	$Q$ (mg g <sup>-1</sup> )	Removal (%)
3.5	2.45	20
8.5	7.29	60
10.5	8.59	71

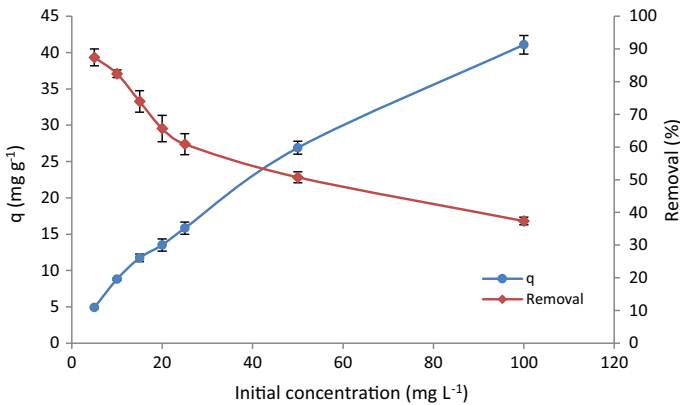


**Fig. 10** Effect of initial concentration on MB adsorption at pH of 10.5, temperature of 25 °C and contact time of 180 min

The pseudo-first-order kinetic model is described with the following formula [29]:

$$\log(q_e - q_t) = \log q_e - \frac{k_{pf}}{2.303} t \quad (3)$$

where  $k_{pf}$  ( $\text{min}^{-1}$ ) is the rate constant of the pseudo-first-order and  $q_t$  ( $\text{mg g}^{-1}$ ) and  $q_e$  ( $\text{mg g}^{-1}$ ) are the amounts of dye adsorbed at time  $t$  (min) and equilibrium, respectively. As shown in Fig. 11a, the values of  $k_1$  and  $q_e$  were determined from the slope and the intercept of the plot.

The pseudo-second-order kinetic model can be exhibited using the following equation [29]:

$$\frac{t}{q_t} = \frac{1}{k_{ps}q_e^2} + \frac{t}{q_e} \quad (4)$$

where  $k_{ps}$  ( $\text{g mg}^{-1} \text{min}^{-1}$ ) is the rate constant of the pseudo-second-order. As shown in Fig. 11b, the values of  $k_{ps}$  and  $q_e$  were determined from the intercept and the slope of the plot.

The following equation can estimate the initial adsorption rate [ $h$  ( $\text{mg g}^{-1} \text{min}^{-1}$ )] for the pseudo-second-order model [30]:

$$h = k_{ps}q_e^2 \quad (5)$$

The intraparticle diffusion model can be expressed using the following equation [31]:

$$q_t = k_p t^{1/2} + C \quad (6)$$

where  $C$  is the intercept and  $k_p$  is the intraparticle diffusion rate constant ( $\text{mg g}^{-1} \text{min}^{-1/2}$ ). They were determined from the intercept and the slope of the plot (Fig. 11c).

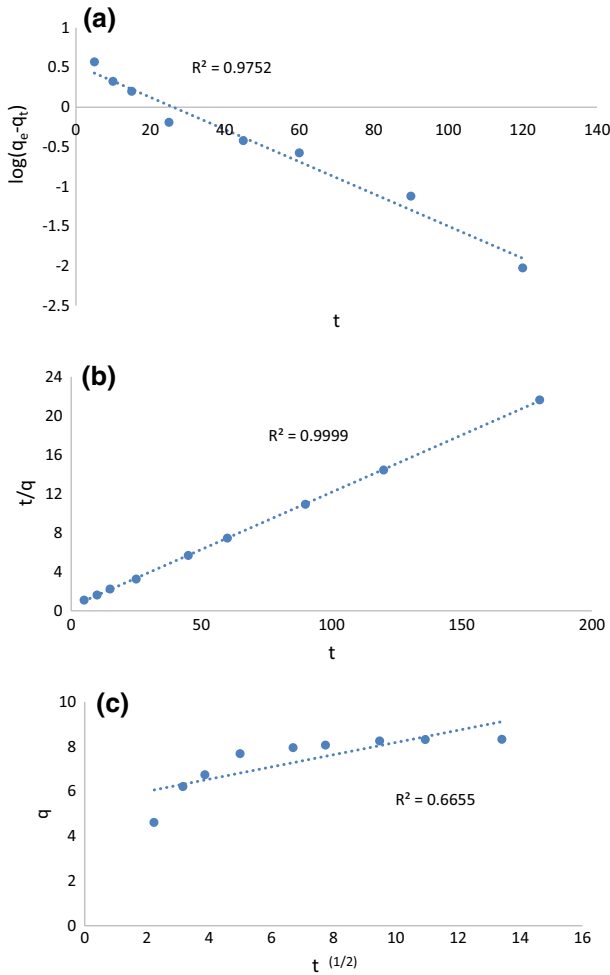


**Fig. 11** Adsorption kinetics of MB adsorbed by MMAs: **a** pseudo-first-order model, **b** pseudo-second-order model, **c** intraparticle diffusion model

The kinetic data were fitted by the kinetic equation models as referred above and arranged in Table 2.

The values of correlation coefficient ( $R^2$ ), which were obtained from the pseudo-second-order kinetics (0.9999) were higher than those obtained from the pseudo-first-order kinetics (0.9752) and the intraparticle diffusion model (0.6655). The values of  $q_{e,2,cal}$  were found to conform well to the experimentally provided data ( $q_{e,exp}$ ). The pseudo-second-order kinetics model which conceivably demonstrates the dye adsorption onto the MMAs is based on the assumption that the rate-limiting step may be chemical sorption or chemisorption involving valency forces through sharing or exchanging electrons between sorbent and sorbate [32].

**Table 2** Adsorption kinetics parameters for MB onto the MMMAs

Experiment	Pseudo-first-order		Pseudo-second-order		Intraparticle model				
	$K_{pf}$ ( $\text{min}^{-1}$ )	$q_{e,1,cal}$ ( $\text{mg g}^{-1}$ )	$R^2$	$K_{ps}$ ( $\text{g mg}^{-1} \text{min}^{-1}$ )	$q_{e,2,cal}$ ( $\text{mg g}^{-1}$ )	$R^2$	$k_{id}$ ( $\text{mg g}^{-1} \text{min}^{-1/2}$ )	$C$ ( $\text{mg g}^{-1}$ )	$R^2$
8.3260	0.0467	3.4103	0.9752	0.0335	8.5251	0.9999	0.2728	5.4537	0.6655

## Adsorption isotherms

In order to determine the adsorption isotherm parameters, three models were used: Langmuir, Freundlich, and Tempkin. To estimate the adsorption parameters of Langmuir isotherm, which presumes the monolayer sorption onto a surface with a limited number of uniform sites, the following formula can be used [33]:

$$\frac{C_e}{q_e} = \frac{C_e}{q_{\max}} + \frac{1}{K_L q_{\max}} \quad (7)$$

where  $q_e$  is the dye concentration onto the adsorbent ( $\text{mg g}^{-1}$ ) at equilibrium and  $q_{\max}$  is the maximum adsorption capacity ( $\text{mg g}^{-1}$ ).  $C_e$  is the dye concentration at equilibrium in the solution ( $\text{mg L}^{-1}$ ).  $K_L$  is the Langmuir constant ( $\text{L mg}^{-1}$ ) related to the tendency of the binding sites and the free energy of adsorption. The slope and the intercept of the plotted straight line ( $C_e/q_e$  vs  $C_e$ ) delineate the values of  $q_{\max}$  and  $K_L$ , respectively (Fig. 12a).

The Langmuir isotherm can be expressed by a constant dimensionless factor specified as the equilibrium parameter ( $R_L$ ):

$$R_L = \frac{1}{1 + K_L C_0} \quad (8)$$

If  $0 < R_L < 1$ , it implies favorable adsorption while  $R_L > 1$ ,  $R_L = 1$  and  $R_L = 0$  infer unfavorable adsorption; linear adsorption and irreversible adsorption process, respectively [30].

The relationship between  $R_L$  and initial MB concentration is illustrated in Fig. 12b. The estimated values of  $R_L$  for all initial concentrations of MB were less than 1 and greater than 0 indicating a favorable adsorption process.

The experimental Freundlich equation for adsorption on a heterogeneous surface is generally expressed using the following formula [34]:

$$\ln q_e = \ln K_F + \frac{1}{n} \ln C_e \quad (9)$$

where  $K_F$  and  $n$  are the Freundlich constants determined by the plotted of  $\ln q_e$  versus  $\ln C_e$  (Fig. 12c).  $K_F$  ( $(\text{mg g}^{-1})/(\text{mg L}^{-1})^{1/n}$ ) refers to the sorption capacity and  $n$  indicates the sorption intensity of the system.

By fitting the experimental data with the Tempkin isotherm model, the enthalpy of adsorption and the adsorbent–adsorbate interactions were evaluated. The Tempkin isotherm equation in linear form can be presented as follows [30]:

$$q_e = \frac{RT}{b_T} \ln K_T + \frac{RT}{b_T} \ln C_e \quad (10)$$

where  $T$  is absolute temperature (K),  $R$  is gas universal constant ( $8.314 \text{ J mol}^{-1} \text{ K}^{-1}$ ),  $b_T$  ( $\text{J mol}^{-1}$ ) is the Tempkin constant related to the enthalpy of adsorption and  $K_T$  ( $\text{L g}^{-1}$ ) is equilibrium binding constant. The Tempkin constants  $b_T$  and  $K_T$  were estimated using the slope and the intercept of the plotted  $q_e$  versus  $\ln C_e$  (Fig. 12d).

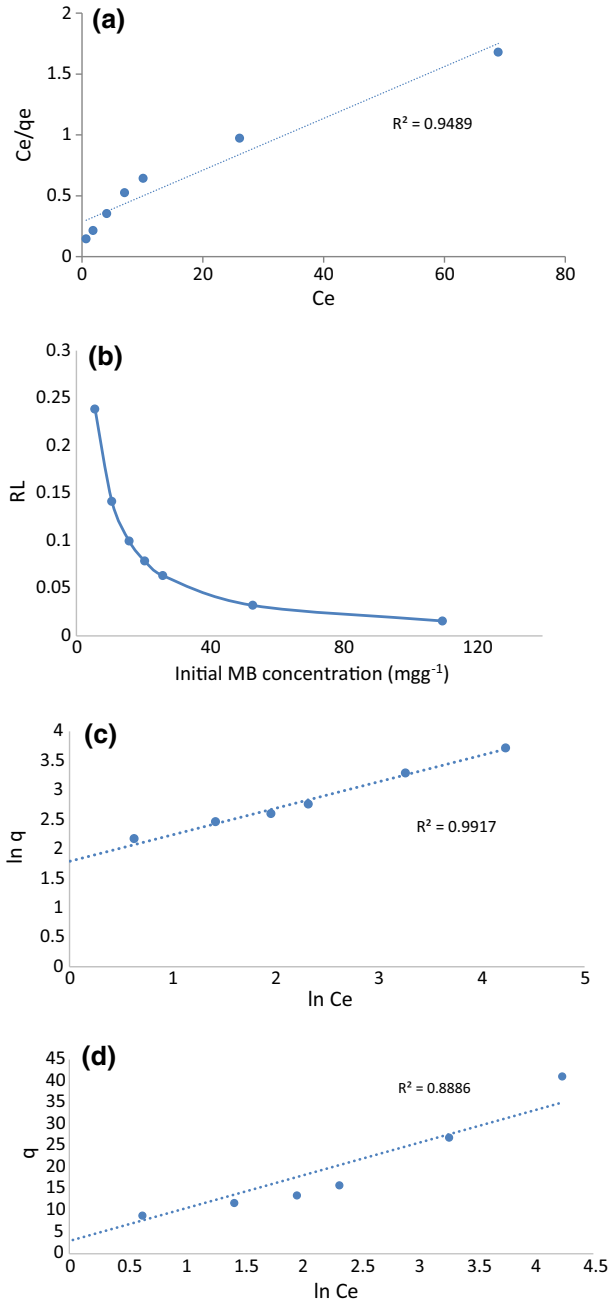


**Fig. 12** Langmuir isotherm (a) and relationship between initial MB concentration and  $R_L$  (b). Freundlich (c) and Temkin (d) isotherms of MB adsorption onto the MMAs



Using these isotherm equations, the adsorption isotherm equilibrium data were calculated and tabulated in Table 3.

The value of  $R^2$  obtained from Freundlich isotherm equation (0.9917) was higher than those obtained from Langmuir (0.9489) and Tempkin (0.8886) isotherm equations. From these observations, it can be concluded that the Freundlich isotherm model, which describes an adsorption process on heterogeneous surface and a multilayer adsorption with interactions between adsorbed molecules, can plausibly verify the MB adsorption on the MMMA. The multi-layer adsorption of MB into the MMMA is based on two interactions, B-MB and MB-MMMA. Interaction between MB and MMMA causes the first layer of adsorption. However, the majority of MB–MB interactions and the minority of MB-MMMA interactions cause adsorption of the other layers in the adsorption process [35].

### Adsorption thermodynamics

Thermodynamics parameters such as the difference in standard Gibbs free energy ( $\Delta G^\circ$ ), enthalpy ( $\Delta H^\circ$ ), and entropy ( $\Delta S^\circ$ ) were calculated for MB adsorption onto the MMMA using the following formulas [36]:

$$K_D = \frac{q_e}{C_e} \quad (11)$$

$$\Delta G^\circ = -RT \ln K_D. \quad (12)$$

$$\ln K_D = \frac{\Delta S^\circ}{R} - \frac{\Delta H^\circ}{RT} \quad (13)$$

The values of  $\Delta H^\circ$  and  $\Delta S^\circ$  were determined from the slope and the intercept of plotted  $\ln K_D$  versus  $1/T$  (Fig. 13) and the standard Gibbs free energy change of sorption ( $\Delta G^\circ$ ) will be evaluated using Eq. 12.

The estimated thermodynamics parameters are arranged in Table 4. The negative values of  $\Delta G^\circ$  at temperatures of 298 and 318 K revealed that the adsorption process is spontaneous at lower temperature, while the positive evaluated data exhibited that the adsorption process becomes non-spontaneous at higher temperature. The negative value of  $\Delta H^\circ$  also indicates an exothermic adsorption process. Furthermore, the negative value of  $\Delta S^\circ$  implies reduction in randomness and increasing in orderliness at the solid/solution interface during the adsorption process [29, 37].

**Table 3** Adsorption isotherm parameters for MB onto the MMMA

Langmuir			Freundlich			Tempkin		
$q_m$ (mg g <sup>-1</sup> )	$K_L$ (L mg <sup>-1</sup> )	$R^2$	$K_F$ (mg/g)(L/ mg) <sup>1/n</sup>	$n$	$R^2$	$b_T$ (J mol <sup>-1</sup> )	$K_T$ (L g <sup>-1</sup> )	$R^2$
46.9484	0.0748	0.9489	5.9864	2.2177	0.9917	365.136	1.4733	0.8886

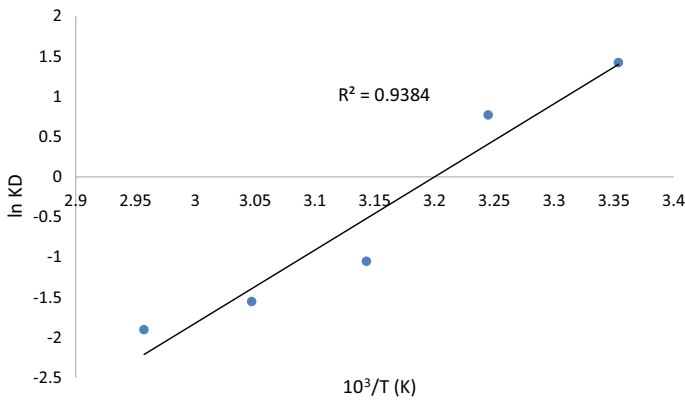


**Fig. 13** Van't Hoff plot for adsorption of MB onto the MMMA

**Table 4** Adsorption thermodynamics parameters for MB onto the MMMA

$\Delta H$ (kJ mol <sup>-1</sup> )	$\Delta S^\circ$ (J mol <sup>-1</sup> K <sup>-1</sup> )	$\Delta G^\circ$ (kJ mol <sup>-1</sup> )				
		298	308	318	328	338
-75.6507	-242.0950	-3.4700	-1.0490	1.3718	3.7928	6.2138

### Comparison of the maximum removal efficiency of MB onto various adsorbents

The maximum removal efficiency of some various adsorbents are presented in Table 5. It should be mentioned that in the most adsorption processes, increasing the adsorbent dosage results in higher removal efficiency. As observed, the 4A/PVA MMA by its specific features exhibits a reasonable dye removal efficiency in the adsorbent dosage of 1 mg L<sup>-1</sup>.

### Conclusion

In this study, the 4A-zeolite/Poly vinyl alcohol mixed matrix membrane adsorbents (MMMA) were prepared by mixing the various contents of 4A-zeolite particles to the PVA. An efficient and applicable adsorption process was achieved due to the effective structure of membrane adsorbent which is caused by adding 4A-zeolite particles. The performance of MMMA improves by increasing the content of 4A-zeolite particles from 5 to 20 wt%. For the sake of an optimum condition in batch adsorption experiments, various experimental parameters were investigated with the adsorbent dosage of 1 g L<sup>-1</sup>. The maximum value of the adsorption capacity ( $q_e$ ) of 41.08 mg g<sup>-1</sup> was gained at temperature of 25 °C, pH of 10.5, MB concentration of 100 mg L<sup>-1</sup> and 20 wt% 4A-zeolite loading and the highest removal efficiency was 87.41 % obtained at temperature of 25 °C, pH of 10.5, initial MB concentration of

**Table 5** Maximum removal efficiency of different adsorbents for MB adsorption

Adsorbent	Adsorbent dosage (g L <sup>-1</sup> )	Maximum removal (%)	Ref.
4A/PVA MMMA	1	87.41	This work
Sapo-34/PVA MMMA	1	89.10	[14]
Keratin nanofibrous membrane	2	97	[24]
Treated animal bone	1.5	90	[38]
PVA	4	~ 87	[25]
Activated carbon from palm stem	0.375	~ 90	[39]
Potato leaves powder	2	~ 85	[40]
Raw ball clay	1	47	[41]
Modified ball clay	1	96	[41]
NaOH-modified malted sorghum mash	40	92.8	[42]
SAC	0.2	~ 95	[43]
GO/CA	0.5	92.7	[34]

5 mg L<sup>-1</sup> and 20 wt% 4A-zeolite loading. Enhancing the MB concentration from 5 to 100 mg L<sup>-1</sup> and pH from 2.5 to 10.5 increases the adsorption capacity, while it decreases at higher temperatures. Equilibrium data were fitted properly with the Freundlich isotherm equation and the rate of MB adsorption on the MMMA conformed the pseudo-second-order rate model. Thermodynamic parameters demonstrated an exothermic adsorption process which is spontaneous and non-spontaneous at lower and higher temperatures, respectively. The MMMA can be introduced as a novel adsorbent for dye removal which supports the simple, environmentally friendly, flexible, and efficient adsorption process.

## References

1. M. Zendehtdel, A. Barati, H. Alikhani, A. Hekmat, Iran. J. Environ. Health Sci. Eng. **7**, 431–436 (2010)
2. X. Zhang, P. Zhang, Z. Wu, L. Zhang, G. Zeng, C. Zhou, Colloids Surf. A **435**, 85–90 (2013)
3. R. Ansari, B. Seyghali, A. Mohammad-khah, M.A. Zanjanchi, Sep. Sci. Technol. **47**, 1802–1812 (2012)
4. S. Haider, F.F. Binagag, A. Haider, A. Mahmood, N. Shah, W.A. Al-Masry, S.U.-D. Khan, S.M. Ramay, Desalination and Water Treatment, 1–11 (2014)
5. P. Kazemi, M. Peydayesh, A. Bandegi, T. Mohammadi, O. Bakhtiari, Chem. Pap. **67**, 722–729 (2013)
6. C. Wang, J. Li, L. Wang, X. Sun, J. Huang, Chin. J. Chem. Eng. **17**, 513–521 (2009)
7. M. Auta, B.H. Hameed, Chem. Eng. J. **237**, 352–361 (2014)
8. J. Fang, X. Huang, X. Ouyang, X. Wang, Chem. Eng. J. **270**, 309–319 (2015)
9. Z.-Y. Zhang, X.-C. Xu, Chem. Eng. J. **256**, 85–92 (2014)
10. C.-H. Lin, C.-H. Gung, J.-Y. Wu, S.-Y. Suen, J. Taiwan Inst. Chem. Eng. **51**, 119–126 (2015)
11. T. Robinson, G. McMullan, R. Marchant, P. Nigam, Bioresour. Technol. **77**, 247–255 (2001)
12. X.S. Wang, Y. Zhou, Y. Jiang, C. Sun, J. Hazard. Mater. **157**, 374–385 (2008)
13. A. Giwa, A. Ogunribido, Brit. J. Appl. Sci. Technol. **2**, 296–310 (2012)

14. R. Ghahremani, B. Baheri, M. Peydayesh, S. Asarehpour, T. Mohammadi, Research on Chemical Intermediates, 1–18 (2015)
15. M. Peydayesh, S. Asarehpour, T. Mohammadi, O. Bakhtiari, Chem. Eng. Res. Des. **91**, 1335–1342 (2013)
16. M. Rezakazemi, A. Ebadi Amooghini, M.M. Montazer-Rahmati, A.F. Ismail, T. Matsuura, Prog. Polym. Sci. **39**, 817–861 (2014)
17. M. Majdan, S. Pikus, M. Kowalska-Ternes, A. Gładysz-Płaska, P. Staszczuk, L. Fuks, H. Skrzypek, J. Colloid Interface Sci. **262**, 321–330 (2003)
18. B. Baheri, M. Shahverdi, M. Rezakazemi, E. Motae, T. Mohammadi, Chem. Eng. Commun. **202**, 316–321 (2014)
19. M. Shahverdi, B. Baheri, M. Rezakazemi, E. Motae, T. Mohammadi, Polym. Eng. Sci. **53**, 1487–1493 (2013)
20. A.A. Kittur, M.Y. Kariduraganavar, U.S. Toti, K. Ramesh, T.M. Aminabhavi, J. Appl. Polym. Sci. **90**, 2441–2448 (2003)
21. S. Shirazian, S. Ghafarnejad Parto, S.N. Ashrafzadeh, Int. J. Appl. Ceram. Technol. **11**, 793–803 (2014)
22. L.R. Rad, A. Momeni, B.F. Ghazani, M. Irani, M. Mahmoudi, B. Noghreh, Chem. Eng. J. **256**, 119–127 (2014)
23. Ş. Sert, C. Kütahyalı, S. İnan, Z. Talip, B. Çetinkaya, M. Eral, Hydrometallurgy **90**, 13–18 (2008)
24. A. Aluigi, F. Rombaldoni, C. Tonetti, L. Jannoke, Study of methylene blue adsorption on keratin nanofibrous membranes. J. Hazard. Mater. **268**, 156–165 (2014)
25. S. Umoren, U. Etim, A. Israel, Adsorption of methylene blue from industrial effluent using poly (vinyl alcohol). J. Mater. Environ. Sci. **4**, 75–86 (2013)
26. L. Jin, Langmuir **18**, 9765–9770 (2002)
27. K.S. Hui, C.Y.H. Chao, S.C. Kot, J. Hazard. Mater. **127**, 89–101 (2005)
28. X. Han, W. Wang, X. Ma, Chem. Eng. J. **171**, 1–8 (2011)
29. J. Zhang, D. Cai, G. Zhang, C. Cai, C. Zhang, G. Qiu, K. Zheng, Z. Wu, Appl. Clay Sci. **83–84**, 137–143 (2013)
30. Y. Liu, Y. Kang, B. Mu, A. Wang, Chem. Eng. J. **237**, 403–410 (2014)
31. Y. Bulut, H. Aydın, Desalination **194**, 259–267 (2006)
32. Y.S. Ho, G. McKay, Process Biochem. **34**, 451–465 (1999)
33. D. Pathania, S. Sharma, P. Singh, Arab. J. Chem. In Press, Corrected Proof (2013)
34. Y. Li, Q. Du, T. Liu, J. Sun, Y. Wang, S. Wu, Z. Wang, Y. Xia, L. Xia, Methylene blue adsorption on graphene oxide/calcium alginate composites. Carbohydr. Polym. **95**, 501–507 (2013)
35. C.-H. Wang, B.J. Hwang, Chem. Eng. Sci. **55**, 4311–4321 (2000)
36. M. Ghaedi, M.D. Ghazanfarkhani, S. Khodadoust, N. Sohrabi, M. Oftade, J. Ind. Eng. Chem. **20**, 2317–2324 (2014)
37. Z. Kong, X. Li, J. Tian, J. Yang, S. Sun, J. Environ. Manage. **134**, 109–116 (2014)
38. A.M.A. Shehata, Removal of methylene blue dye from aqueous solutions by using treated animal bone as a cheap natural adsorbent. Int. J. Emerg. Technol. Adv. Eng. **3**, 1–7 (2013)
39. Z.A. AlOthman, M.A. Habila, R. Ali, A.A. Ghafar, M.S.E. Hassouna, Valorization of two waste streams into activated carbon and studying its adsorption kinetics, equilibrium isotherms, and thermodynamics for methylene blue removal. Arab. J. Chem. (2013)
40. N. Gupta, A.K. Kushwaha, M.C. Chattopadhyaya, Application of potato (*Solanum tuberosum*) plant wastes for the removal of methylene blue and malachite green dye from aqueous solution. Arab. J. Chem. (2011)
41. M. Auta, B.H. Hameed, Modified mesoporous clay adsorbent for adsorption isotherm and kinetics of methylene blue. Chem. Eng. J. **198–199**, 219–227 (2012)
42. E.O. Oyelude, F. Appiah-Takyi, Removal of methylene blue from aqueous solution using alkali-modified malted sorghum mash. Turk. J. Eng. Environ. Sci. **36**, 161–169 (2012)
43. C.H. Weng, Y. Pan, Adsorption of a cationic dye (methylene blue) onto spent activated clay. J. Hazard. Mater. **144**, 355–362 (2007)